

## Breakdown of chiral symmetry during saturation of the Tayler instability

Alfio Bonanno,<sup>1,2</sup> Axel Brandenburg,<sup>3,4</sup> Fabio Del Sordo,<sup>3,4</sup> and Dhrubaditya Mitra<sup>3</sup>

<sup>1</sup>*INAF, Osservatorio Astrofisico di Catania, Via S. Sofia 78, 95123 Catania, Italy*

<sup>2</sup>*INFN, Sezione di Catania, Via S. Sofia 72, 95123 Catania, Italy*

<sup>3</sup>*Nordita, Royal Institute of Technology and Stockholm University, Roslagstullsbacken 23, SE-10691 Stockholm, Sweden*

<sup>4</sup>*Department of Astronomy, Stockholm University, SE 10691 Stockholm, Sweden*

(Received 30 March 2012; published 13 July 2012)

We study spontaneous breakdown of chiral symmetry during the nonlinear evolution of the Tayler instability. We start with an initial steady state of zero helicity. Within linearized perturbation calculations, helical perturbations of this initial state have the same growth rate for either sign of helicity. Direct numerical simulations (DNS) of the fully nonlinear equations, however, show that an infinitesimal excess of one sign of helicity in the initial perturbation gives rise to a saturated helical state. We further show that this symmetry breaking can be described by weakly nonlinear finite-amplitude equations with undetermined coefficients which can be deduced solely from symmetry consideration. By fitting solutions of the amplitude equations to data from DNS, we further determine the coefficients of the amplitude equations.

DOI: [10.1103/PhysRevE.86.016313](https://doi.org/10.1103/PhysRevE.86.016313)

PACS number(s): 47.20.Bp, 52.35.Py, 11.30.Qc, 07.55.Db

### I. INTRODUCTION

There are many examples in nature where the ground state does not share the same symmetries of the underlying equations of motion [1]. The most common examples include equilibrium phase transition, e.g., the case of a liquid-solid transition where the space translational symmetry is broken, or that of a paramagnetic-ferromagnetic transition where the spin-rotational symmetry is broken; see, e.g., Ref. [2] for a detailed discussion. However, the original symmetry is not lost but gives rise to the appearance of a regular structure with a specific length scale.

In nonequilibrium physics, spontaneous symmetry breaking is often observed when some control parameter is increased above a critical value; see, e.g., Ref. [3] for a comprehensive introduction. Two well-studied examples from fluid dynamics include the case of Rayleigh-Bénard convection [3] and the Mullins-Sekerka instability of a moving interface between two phases [4]. These systems, too, are invariant under translation and reflection, but the basic instability produces a symmetry-breaking bifurcation in which the continuous translational symmetry of the basic state is broken to a discrete one, although the mirror symmetry is often retained. If the instability parameter is raised further, secondary instabilities may break the periodic pattern and eventually a completely new symmetry-broken state may emerge, as has been seen in several experiments [5]. At very high values of the control parameter, turbulence sets in and most of the symmetries are statistically restored.

In a hydrodynamic system under rotation, spontaneous breakdown of chiral symmetry has been studied; see, e.g., Ref. [7]. Spontaneous chiral symmetry breaking is also found in liquid crystals [6]. Preliminary evidence showing spontaneous chiral symmetry breaking in magnetohydrodynamics (MHD), in the absence of rotation, has been presented for the magnetic buoyancy instability [8] and for the Tayler instability in a Taylor-Couette setup [9]. However, the role of the dynamics of the bifurcation process is still poorly understood.

The purpose of the present paper is twofold. First we demonstrate the occurrence of spontaneous chiral symmetry

breaking in the context of a global instability of the toroidal field, and second we elucidate some aspects of the underlying nonlinear mechanism which determines the evolution from a mirror-symmetric state to a state with a preferred handedness or helicity. In particular, we shall be interested in the case of the Tayler instability [10,11], which has attracted much interest in recent times for its possible astrophysical applications [9,12–18]. We thus discuss the possibility of generating a final state with finite helicity starting from a nonhelical basic state, using a very small controlled helical perturbation.

Our setup has the advantage of better clarifying the complex nonlinear coupling between the different modes, which eventually leads to the formation of a final helical state. In fact, the Tayler instability, in its simplest realization, has no threshold field, at least in ideal MHD [13], where a sufficient condition for instability simply reads

$$\beta \equiv \frac{\partial \ln B_\varphi}{\partial \ln s} > -\frac{1}{2}, \quad (1)$$

$s$  being the cylindrical radius. On the other hand, the spectrum is characterized by an infinite number of unstable modes all characterized by pairs of opposite azimuthal wave number  $m = \pm 1, 2, 3, \dots$ , but with precisely the same growth rate. In particular, as is well known,  $m = \pm 1$  are the modes with the fastest growth rate. Here our aim is to understand the dynamics of the bifurcation process which leads to the selection of a final state of finite helicity and to understand the evolution of the system after the bifurcation takes place. It should also be noted that in the linear stage, the preferred helicity is determined essentially by the helicity of the perturbation, but the nonlinear evolution can be rather complex and it is not clear *a priori* what the final selected helical state would be.

The rest of the paper is organized as follows. In Sec. II, we write down the finite-amplitude equations that govern the evolution of the instability in the weakly nonlinear phase. Our approach is based on symmetry arguments; a detailed analytical derivation of the amplitude equations is avoided here. We find that the amplitude equations predict a breakdown of parity for a certain choice of parameters. Direct numerical

simulations (DNS) of the fully nonlinear equations describing the evolution of the Taylor instability are performed in Sec. III. In our DNS studies, we also find breakdown of parity. We fit data from DNS to solutions of the amplitude equations to numerically determine the parameters appearing in the amplitude equations. It turns out that the amplitude equations we deduce are identical to those used to describe the breakdown of mirror symmetry in studies of the biochemical origin of life. This connection is explored in Sec. IV. Finally, conclusions are drawn in Sec. V

## II. AMPLITUDE EQUATIONS

To the best of our knowledge, the amplitude equations describing the spontaneous breakdown of mirror symmetry in hydrodynamic instabilities were first described in Ref. [19]. The basic idea is as follows.

Let us consider an instability with two growing modes with opposite helicity but exactly the same growth rate and let the amplitude in this basis of the left- and right-handed modes be given by vectors  $\hat{\mathbf{L}}$  and  $\hat{\mathbf{R}}$ , respectively. In physical space, we have

$$\mathbf{L}(\mathbf{x}) = \hat{\mathbf{L}}\phi(\mathbf{n}), \quad (2)$$

$$\mathbf{R}(\mathbf{x}) = \hat{\mathbf{R}}\phi(\mathbf{n}). \quad (3)$$

For example, in Cartesian domains, with real-space coordinate  $\mathbf{x}$ ,  $\phi(\mathbf{n}) = \exp(i\mathbf{n} \cdot \mathbf{x})$ . In cylindrical coordinate,  $\phi$  is a combination of trigonometric and Bessel functions. As the modes are helical, they satisfy the Beltrami relation,

$$\nabla \times \mathbf{R} = \Lambda \mathbf{R} \quad \text{and} \quad \nabla \times \mathbf{L} = -\Lambda \mathbf{L}. \quad (4)$$

For the present problem, explicit expressions involve a linear combinations of the type  $J_m(s\sqrt{\Lambda^2 + n^2\pi^2/h^2})\cos(m\phi)\cos(zn\pi/h)$ , where  $J_m$  is the Bessel function of the first kind,  $n, m = \pm 1, 2, 3 \dots$ ,  $h$  is the height of the cylinder, and  $s$  the cylindrical radius [20]. The set of such modes forms a complete set (a Hilbert basis) for the spatial distribution of the field.

Here we assume that the dynamical evolution of the unstable mode is determined by an effective Lagrangian. For the left-handed helical mode, total helicity and energy are given by

$$E_L = \frac{1}{2} \int \mathbf{L}^2(\mathbf{x}) d^3x = \frac{1}{2} \hat{\mathbf{L}} \cdot \hat{\mathbf{L}}^*, \quad (5)$$

$$\mathcal{H}_L = \int \mathbf{L} \cdot \nabla \times \mathbf{L} d^3x = -2\Lambda E_L, \quad (6)$$

where an asterisk denotes complex conjugation. Analogous definitions apply also to  $E_R$  and  $\mathcal{H}_R = +2\Lambda E_R$ . We then have  $E = E_L + E_R$  being the total energy and  $\mathcal{H} = \mathcal{H}_L + \mathcal{H}_R$  the total helicity. In the weakly nonlinear regime, the amplitude equations can be written as

$$\frac{\partial \hat{\mathbf{L}}}{\partial t} = \frac{\delta \mathcal{L}}{\delta \hat{\mathbf{L}}} \quad \text{and} \quad \frac{\partial \hat{\mathbf{R}}}{\partial t} = \frac{\delta \mathcal{L}}{\delta \hat{\mathbf{R}}}, \quad (7)$$

where the simplest form of the Lagrangian is given by

$$\mathcal{L}[\hat{\mathbf{L}}, \hat{\mathbf{R}}] = \gamma[|\hat{\mathbf{L}}|^2 + |\hat{\mathbf{R}}|^2] - \mu[|\hat{\mathbf{L}}|^4 + |\hat{\mathbf{R}}|^4]. \quad (8)$$

The form of the Lagrangian is determined by the symmetry of the problem. The coefficient  $\gamma$  is the linear growth rate and

$\mu$  determines the saturation of the instability in the weakly nonlinear regime. We emphasize that the  $\mu$  and  $\gamma$  for  $\hat{\mathbf{L}}$  and  $\hat{\mathbf{R}}$  could be different if and only if the chiral symmetry is broken from the outset, but this is *not* the case here. Now note that the Lagrangian must also be invariant under the parity transformation, under which

$$\mathcal{P}(\hat{\mathbf{L}}) = \hat{\mathbf{R}} \quad \text{and} \quad \mathcal{P}(\hat{\mathbf{R}}) = \hat{\mathbf{L}}. \quad (9)$$

This additional symmetry allows one additional term in the Lagrangian given by

$$-\mu_*(|\hat{\mathbf{L}}|^2|\hat{\mathbf{R}}|^2). \quad (10)$$

With this additional term in the Lagrangian, the evolution equations for the two eigenmodes are given by

$$\frac{\partial \hat{\mathbf{L}}}{\partial t} = \gamma \hat{\mathbf{L}} - (\mu|\hat{\mathbf{L}}|^2 + \mu_*|\hat{\mathbf{R}}|^2)\hat{\mathbf{L}}, \quad (11a)$$

$$\frac{\partial \hat{\mathbf{R}}}{\partial t} = \gamma \hat{\mathbf{R}} - (\mu|\hat{\mathbf{R}}|^2 + \mu_*|\hat{\mathbf{L}}|^2)\hat{\mathbf{R}}. \quad (11b)$$

These equations, for certain parameters, allow and can describe the growth of one handedness while the other is extinguished [19]. Similar equations, which describe the time dependence of the amplitudes of the leading modes, but without considering their spatial dependence, are often used to extend linear perturbation theory of hydrodynamic instabilities into the weakly nonlinear regime. In this form, they are often called the Landau equations [21].

The energy of the left- and right-handed modes is determined by

$$\frac{dE_L}{dt} = 2\gamma E_L - 4\mu E_L^2 - 4\mu_* E_L E_R, \quad (12a)$$

$$\frac{dE_R}{dt} = 2\gamma E_R - 4\mu E_R^2 - 4\mu_* E_L E_R. \quad (12b)$$

These equations show that both  $E_L$  and  $E_R$  grow exponentially at the rate  $2\gamma$  until nonlinear effects become important and either  $E_L$  or  $E_R$  saturates at  $E_0 \equiv \gamma/2\mu$  and the energy of the mode of opposite handedness vanishes. In principle, the achiral solution with  $E_L = E_R \equiv E_a = \gamma/2(\mu + \mu_*)$  is also possible, but, as we will see below, such a solution is unstable for  $\mu < \mu_*$ , which is what we find in Sec. III. The reason for this instability is the presence of the term proportional to  $\mu_*$ , which represents a phenomenon known as ‘‘mutual antagonism’’ in studies of the origin of homochirality of biomolecules [22–24]. We will return to this issue in Sec. IV, where we discuss the analogy with chiral symmetry breaking in biomolecules in more detail.

Using Eqs. (6) and (11) and defining  $H = \mathcal{H}/2\Lambda$ , we have  $E_R = (E + H)/2$  and  $E_L = (E - H)/2$ . We can thus obtain the following evolution equations:

$$\frac{dE}{dt} = 2\gamma E - 2(\mu + \mu_*)E^2 - 2(\mu - \mu_*)H^2, \quad (13a)$$

$$\frac{dH}{dt} = 2\gamma H - 4\mu EH. \quad (13b)$$

The dynamical system described by (13) and depicted in Fig. 1 has four fixed points in the  $(E, H)$  plane:  $S_1 = (0, 0)$ ,  $S_{2,3} = (E_0, \pm E_0)$ , and  $S_4 = (2E_a, 0)$  with eigenvalues  $\lambda_1 = (2\gamma, 2\gamma)$ ,  $\lambda_2 = \lambda_3 = (-2\gamma, 2(\mu - \mu_*)/\gamma)$ , and  $\lambda_4 =$

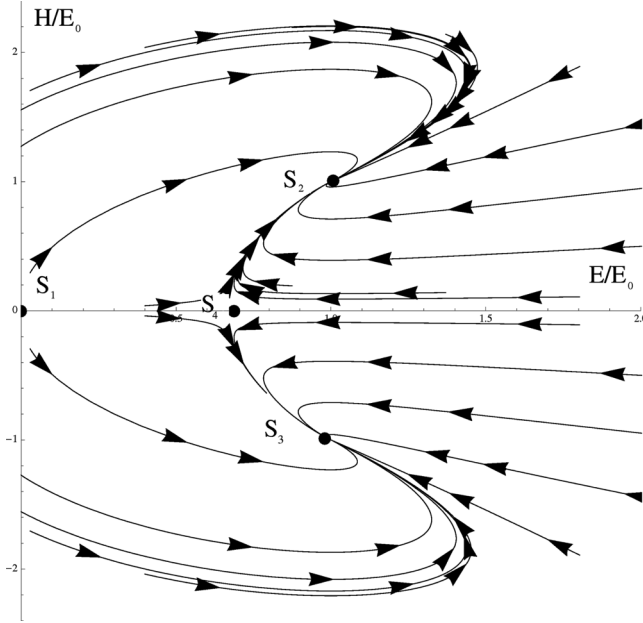


FIG. 1. The phase portrait for  $\mu < \mu_*$ . This is the typical situation in which  $S_2$  and  $S_3$  are attractive and  $S_4$  is a saddle point.

( $-2\gamma, 2\gamma - 4\gamma\mu/(\mu + \mu_*)$ ). The origin is always repulsive while  $S_2$  and  $S_3$  are sinks or saddle points depending on the values of parameters  $\mu$  and  $\mu_*$ .  $S_4$ , corresponding to the achiral solution, can be an attractive point only if  $\mu_* < \mu$ , otherwise it is a saddle point.

A discussion of the amplitude equations is now in order. First, we have assumed that there are exactly two modes of opposite helicity that becomes critical at the onset of the instability. This assumption is based on linear perturbation analysis. As all the other modes in this case are stable, in the spirit of center manifold reduction, we have ignored their contributions to total energy and helicity. If several modes are simultaneously unstable at the onset, then we may expect a higher degree of complexity. Secondly, as our approach is based on symmetry, the form of the amplitude equations that we obtain is very general. This is also a weakness of our approach, as we cannot determine the expression for either  $\mu$  or  $\mu_*$ . In principle, the method of multiscale expansion or center manifold reduction can be applied to this problem to derive an analytical expression of  $\mu$  and  $\mu_*$ , but this is a difficult proposition in the present case as a solution of the linear problem itself is not known in an analytically closed form.

We can then compute the quantities  $\gamma$ ,  $\mu$ , and  $\mu_*$  with the help of DNS by comparing the time evolution obtained for the left-hand side of (13) in the weakly nonlinear phase where our description is valid. We can anticipate that in most of our simulations,  $\mu < \mu_*$  and therefore the system should relax to a state of finite helicity in a finite time, although we start from an infinitesimally small helicity. This is precisely what we observe in our DNS.

### III. DIRECT NUMERICAL SIMULATIONS

To analyze the evolution of the Tayler instability, we choose our numerical domain to be a cylindrical shell with an inner

radius  $s_{\text{in}} = 1$ , outer radius  $s_{\text{out}} = 3$ , and height  $h = 2$ . We perform simulations of the time-dependent resistive magnetohydrodynamic equations for a compressible isothermal gas: the pressure is thus given by  $p = \rho c_s^2$ , where  $\rho$  is the density and  $c_s$  is the isothermal sound speed.

We use the PENCIL CODE<sup>1</sup> to solve the equations for the magnetic vector potential  $\mathbf{A}$ , ( $\mathbf{B} = \nabla \times \mathbf{A}$ ) the velocity  $\mathbf{U}$ , and the logarithmic density  $\ln \rho$  in the form

$$\frac{\partial \mathbf{A}}{\partial t} = \mathbf{U} \times \mathbf{B} + \eta \nabla^2 \mathbf{A}, \quad (14)$$

$$\frac{D\mathbf{U}}{Dt} = -c_s^2 \nabla \ln \rho + \mathbf{J} \times \mathbf{B} / \rho + \mathbf{F}_{\text{visc}}, \quad (15)$$

$$\frac{D \ln \rho}{Dt} = -\nabla \cdot \mathbf{U}, \quad (16)$$

where

$$\mathbf{F}_{\text{visc}} = \rho^{-1} \nabla \cdot 2\nu \rho \mathbf{S}$$

is the viscous force,  $\mathbf{S}$  is the traceless rate of strain tensor having components  $S_{ij} = \frac{1}{2}(U_{i,j} + U_{j,i}) - \frac{1}{3}\delta_{ij} \nabla \cdot \mathbf{U}$ ,

$$\mathbf{J} = \nabla \times \mathbf{B} / \mu_0$$

is the current density,  $\nu$  is the kinematic viscosity, and  $\eta$  is the magnetic diffusivity.

We choose periodic boundary conditions in the vertical ( $z$ ) and azimuthal ( $\varphi$ ) directions, while at radial ( $s$ ) boundaries we select a perfectly conducting boundary condition for the magnetic field and stress-free boundary conditions for velocity. The resolution of the simulations presented here is  $128^3$  mesh points in all three directions, but comparison with different resolution demonstrated that our results are converged.

We choose a basic state with zero velocity and zero axial component of the magnetic field ( $B_z$ ). The azimuthal component of the magnetic field is

$$B_\varphi = B_0 (s/s_0) \exp[-(s - s_0)^2/\sigma^2], \quad (17)$$

where  $B_0$  is a normalization constant,  $s_0 = 2$ , and  $\sigma = 0.2$ . We choose  $B_0$  and  $c_s$  in such a way that the sound speed is much larger than the Alfvén speed. In this way, we avoid magnetic perturbation to be dominant over hydrodynamical perturbations.

In the basic state, the Lorentz force due to the magnetic field is balanced by the gradient of pressure. Hence the pressure of the fluid is given by

$$p = p_0 - \frac{B_0^2}{4s_0^2} \left[ (2s^2 - \sigma^2) e^{-\frac{(s-s_0)^2}{\sigma^2}} + s_0 \sigma \sqrt{\pi} \sqrt{2} \operatorname{erf} \left( \frac{\sqrt{2}(s-s_0)}{\sigma} \right) \right], \quad (18)$$

where  $p_0$  is a constant that must be large enough to ensure that the pressure is positive. If no perturbation is added, the system remains stationary. Therefore, we add at the beginning of the simulation a perturbation of the magnetic field with an infinitesimally small net helicity given by the following

<sup>1</sup><http://pencil-code.googlecode.com/>

expression:

$$\mathbf{A} = \delta s \cos\left(z \frac{n_z \pi}{h}\right) \begin{pmatrix} \sin m\varphi \\ 0 \\ \cos m\varphi \end{pmatrix}, \quad (19)$$

where  $\delta$  is an arbitrary small amplitude which we set to  $10^{-7}$  for all the simulations and  $k_z = q/s_{\text{in}} = n_z \pi/h$  is the vertical wave number of the perturbation.

As discussed in [13], kink instabilities are a special case of the so-called quasi-interchange instabilities, where combined azimuthal and vertical fields are present in the basic state. In the incompressible limit, the unstable eigenmodes can be described by a  $(t, z, \varphi)$  dependence of the type  $\propto \exp(\gamma t - ik_z z - im\varphi)$  where the growth rate  $\gamma$  is determined from a numerical solution of the nonlinear eigenvalue problem for the radial disturbance  $v_{1s}$ ,

$$\begin{aligned} \frac{d}{ds} \left[ \frac{1}{\lambda} (\gamma^2 + \omega_A^2) \left( \frac{dv_{1s}}{ds} + \frac{v_{1s}}{s} \right) \right] - k_z^2 (\gamma^2 + \omega_A^2) v_{1s} \\ + 2\omega_B \left[ \frac{m(1+\lambda)}{s^2 \lambda^2} \left( 1 - \frac{\beta \lambda}{1+\lambda} \right) (\omega_{Az} + 2m\omega_B) \right. \\ \left. + \frac{m\omega_{Az}}{s^2 \lambda^2} - k_z^2 \omega_B (1-\beta) \right] v_{1s} + \frac{4k_z^2 \omega_A^2 \omega_B^2}{\lambda(\gamma^2 + \omega_A^2)} v_{1s} = 0. \end{aligned} \quad (20)$$

Here  $\omega_A = (\mathbf{B} \cdot \mathbf{k})/\sqrt{\rho}$  with  $\mathbf{k} = (0, m/s, k_z)$ , so  $\omega_{Az} = k_z B_z/\sqrt{\rho}$ . Furthermore, we have defined  $\omega_B = B_\varphi/s\sqrt{\rho}$  and  $\lambda = 1 + m^2/s^2 k_z^2$ .

Equation (20) describes the stability problem as a nonlinear eigenvalue problem. This equation was first derived by Freidberg [25] in his study of MHD stability of a diffuse screw pinch (see also [13]). The author found that, for a given value of  $k_z$ , it is possible to obtain multiple values of the eigenvalue  $\gamma$ , each one corresponding to a different eigenfunction, and he calculated  $\gamma$  for the fastest growing fundamental mode. The most general form of Eq. (20), taking into account compressibility of plasma, was derived by Goedbloed [26]. Since we study the stability assuming that the magnetic energy is smaller than the thermal energy, the incompressible form of Eq. (20) can be a sufficiently accurate approximation, as we have verified. In the case at hand,  $(\mathbf{B} \cdot \mathbf{k})/\sqrt{\rho} = m\omega_B = \omega_A$  because we are interested in pure kink (Taylor) instabilities, with  $B_z \equiv 0$  in the basic state. Note that as  $\omega_{Az} = 0$  in our case, Eq. (20) is invariant for  $m \rightarrow -m$ .

In this latter case, once (20) is solved and  $v_{1s}$  is obtained, the expressions for the other perturbed quantities denoted by the subscript “1” read

$$B_{1s} = -\frac{i}{\gamma s} B_\varphi v_{1s}, \quad (21a)$$

$$B_{1\varphi} = -\frac{i}{\gamma s} B_\varphi v_{1\varphi} - \frac{B_\varphi}{\gamma s} (\beta - 1) v_{1s}, \quad (21b)$$

$$B_{1z} = -\frac{i}{\gamma s} B_\varphi v_{1z}, \quad (21c)$$

$$v_{1\varphi} = \frac{-im}{(k_z s)^2 \lambda} \frac{\partial}{\partial s} (s v_{1s}) - \frac{2im\omega_B^2 v_{1s}}{\lambda(\gamma^2 + m^2 \omega_B^2)}, \quad (21d)$$

$$v_{1z} = -\frac{i}{k_z s} \frac{\partial}{\partial s} (s v_{1s}) - \frac{m}{k_z s} v_{1\varphi}. \quad (21e)$$

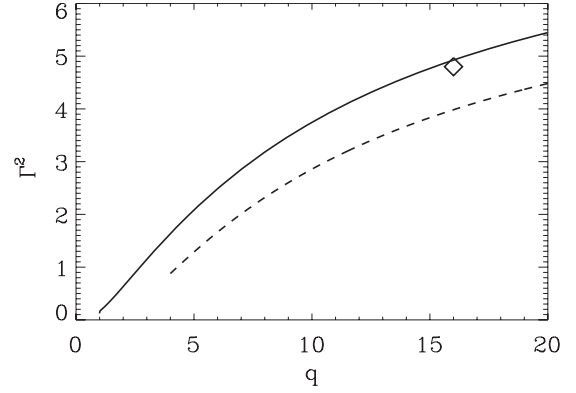


FIG. 2. The dispersion relation for the dimensionless growth rate  $\Gamma$  for the  $m = \pm 1$  mode (solid line) and for the  $m = \pm 2$  mode (dashed). Higher values of  $|m|$  have even smaller growth rates. This curve is obtained for a linear model with physical parameters corresponding to the nonlinear model He1d, for which we indicate, with a rhombus, the growth rate for its faster growing mode.

Unfortunately even for the case of pure kink instabilities, (20) cannot be solved analytically and one has to determine the dispersion relation numerically. Therefore, to test our numerical setup we have solved numerically Eq. (20) for the basic state (17) for various values of  $B_0$  and  $\sigma$  in the limit of small  $v_A/c_s$  ratio to check that in the linear phase the growth rate extracted from the DNS is in agreement with the linear theory. In particular, as the inner radius of the cylinder is not at  $s = 0$ , we have set  $v_{1s} = 0$  at both inner and outer boundaries. Note here that the growth rate and eigenfunctions of this instability are known for the ideal MHD limit. Hence to compare with those results, we choose viscosity and magnetic diffusivity such that the dissipative time scales are much larger than the characteristic growth time (inverse of  $\gamma$ ) of the instability.

The results are shown in Fig. 2 for the dimensionless growth rate  $\Gamma = \gamma t_A$ , where  $t_A = s_{\text{out}} \sqrt{\rho}/B_0$  is the Alfvén travel time, as a function of the dimensionless vertical wave number  $q = k_z s_{\text{in}}$  for model He1d in Table I, with  $B_0 = 0.5$ , and  $n_z = 10$ . In particular, to compare the growth rate obtained from our DNS, we have determined the characteristic vertical wave number of the unstable mode in the linear phase by means of the Fourier analysis of the magnetic fields. We also found that in all the simulations, the azimuthal wave number of the fastest growing mode turned out to be always  $m = \pm 1$  as higher values of  $|m|$  have a smaller growth rate (as shown in Fig. 2). We found that the corresponding growth rate determined from the linear phase of our direct numerical simulation is about 7–5 % smaller than the linear value. We think this is acceptable in view of unavoidable numerical diffusion in three-dimensional numerical simulations.

We see that the eigenfunction is rather localized for  $q \gg 1$ , as is visible in the example shown in Fig. 3. We can exploit this property to obtain approximate explicit expressions for the growth rate at large values of  $q$ . In fact, we can consider the magnetic field approximately constant around  $s = s_0$  and apply the small-gap approximation (see [13] for details) so that  $v_{1s} \propto \sin[\pi(s - s_0)/\sigma]$  and the dimensionless growth rate

TABLE I. For every model,  $s$  goes from 1 to 3,  $z$  from  $-1$  to 1, and the perturbation has an amplitude  $\delta = 10^{-7}$ ,  $\sigma = 0.2$ .

Model	$B_0^2/p_0$	$v_A/c_s$	$c_s$	$m$	$n_z$	$\gamma t_A$	$\mu \frac{s_{\text{out}}^2}{t_A}$	$\mu_* \frac{s_{\text{out}}^2}{t_A}$	$\mu_*/\mu$
Hel	$10^{-1}$	0.3	10	$-1$	1	2.71	7.5	18	2.4
Helm1	$10^{-1}$	0.3	10	$+1$	1	2.71	7.5	18	2.4
Helc	$10^{-1}$	0.3	20	$-1$	1	6.2	7	18.5	2.6
Helmb	$2.5 \times 10^{-2}$	0.15	10	$-1$	1	2.2	1	2.3	2.3
Held	$2.5 \times 10^{-2}$	0.15	10	$-1$	10	2.2	3	7.3	2.4
Heln10	$10^{-1}$	0.3	10	$-1$	10	2.75	4.5	10	2.2

reads

$$\Gamma^2 = -\frac{2c\Delta^2 m^2[(\beta - 1)m^2 + (\beta - 3)q^2]}{(m^2 + q^2)[\Delta^2(m^2 + q^2) + \pi^2]} + \frac{2(\beta - 1)\Delta^2 q^2 - c^2 m^2[\Delta^2(m^2 - 3q^2) + \pi^2]}{\Delta^2(m^2 + q^2) + \pi^2}, \quad (22)$$

where  $c = B_\phi/B_0 \approx \text{const}$  and  $\Delta = 2\sigma/s_0$ . In the limit  $q \gg 1$ , despite the uncertain approximation that we have performed, expression (23) differs by only 20% from the numerical solution.

It is interesting to notice that, by using (21) in the limit  $q \gg 1$ , we obtain the explicit expressions

$$\langle \mathbf{v}_1 \cdot \nabla \times \mathbf{v}_1 \rangle \approx -\frac{4m\omega_B^2(\gamma^2 - m^2\omega_B^2)\langle v_{1s}^2 \rangle}{s_0^2 k_z (\gamma^2 + m^2\omega_B^2)^2}, \quad (23)$$

$$\langle \mathbf{B}_1 \cdot \nabla \times \mathbf{B}_1 \rangle \approx \frac{4mB_\phi^2\omega_B^2\langle v_{1s}^2 \rangle}{s_0^4 k_z (\gamma^2 + m^2\omega_B^2)^2}, \quad (24)$$

where the symbol  $\langle \cdot \rangle$  denotes volume averaging. It is therefore clear that, at the nonlinear level, eigenfunctions with nonzero  $m$  will produce both kinetic and magnetic helicity whose sign will depend on the sign of  $m$ . The relevant point is that modes with opposite  $m$  have an identical growth rate but opposite

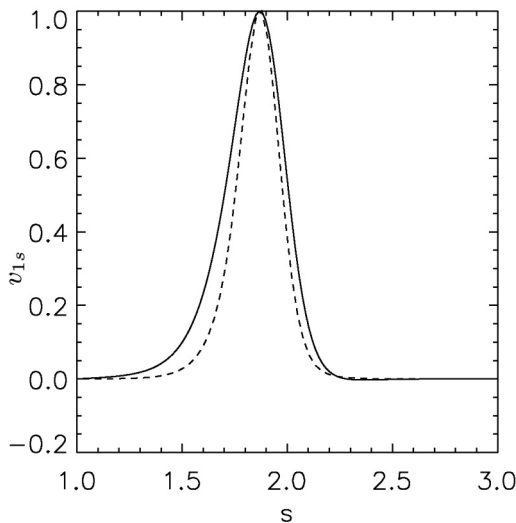


FIG. 3. Eigenfunction  $v_{1s}$  for the  $m = 1$  mode for  $q = 16$ . The result of the simulation, model HelD in Table I (solid line), is overplotted on the eigenfunction obtained solving (20) (dashed line); see [13] for more details. This is observed at  $t/t_A = 9$ , that is, during the linear growth of the instability.

kinetic and magnetic helicity, and the fate of the final helicity is decided by the competition of modes with opposite azimuthal wave number.

Moreover, according to the oscillation theorem [27], as the  $m = \pm 1$  are unstable, all the other modes with  $m = \pm a$ , where  $a > 1$  is a positive integer, are also unstable, but with a smaller growth rate. As a consequence, although in the linear phase the  $m = \pm 1$  modes dominate the linear growth, already in the weakly nonlinear phase the contribution of modes with  $m \neq \pm 1$  can also be important for the selection of the final helical state.

The eigenfunctions appear clearly in our simulation and they fit quite well the eigenfunctions calculated by the linear model, as shown in Fig. 3. In our simulations, during the growing phase of the instability we observe a net increase of the helicity, as shown in Fig. 4, where we plot the time series of the normalized kinetic, current, and magnetic helicity. It is interesting to notice that while kinetic helicity decays on the viscous time scale, the current and magnetic helicities reach a nonzero value at very large times.

In actual simulations, we choose  $\nu = 10^{-2}$  (in code units) so that the viscous time scale is  $t_\nu = s^2/\nu \gg \gamma^{-1}$  and the actual value of  $\nu$  does not play a significant role in the weakly nonlinear phase, as we verified in our simulations. Moreover, we decided to use a very small value for the magnetic diffusivity,  $\eta = 10^{-9}$  (in code units). This is done to prevent the decay of the magnetic field by diffusion. In general, such small values of magnetic diffusivity would imply extremely large values of the magnetic Reynolds number which would be impossible to resolve with the resolutions we use. Nevertheless, we choose such values to have a toroidal field stable on time scales much longer than those of the instability. However, in our simulations no sharp gradients of the magnetic field develop, which is the reason why such small values of magnetic diffusivity are permissible.

We can now determine the coefficients  $\gamma$ ,  $\mu$ , and  $\mu_*$  using the time evolution of  $H(t)$  and  $E(t)$  obtained with our DNS in solving the model (13). This can be done via a direct two-parameter  $\chi^2$  minimization because the exponent  $\gamma$  can easily be determined from the linear evolution and one is left with only the determination of  $\mu$  and  $\mu_*$ . An example of this approach is depicted in Fig. 5, where the agreement with our numerical simulations is explicitly shown. Note that around  $t/t_A \approx 6.5$  we enter the deep nonlinear phase and our treatment does not apply anymore. We estimate this cutoff time for our simulations to be in the middle of the decay transition for  $d \ln H/dt$  and  $d \ln E/dt$  depicted in Fig. 5, and we have checked that the values of  $\mu$  and  $\mu_*$  are not strongly dependent on our cutoff time.

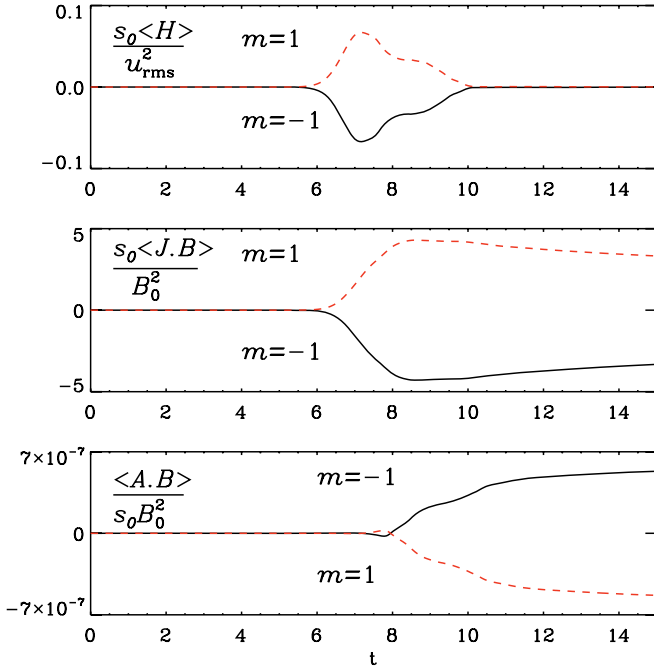


FIG. 4. (Color online) Kinetic, current, and magnetic helicities for two different runs (models He1 and He1m1 in Table I) with helical perturbation and  $m = \pm 1$ .  $t$  is in units of the Alfvén travel time  $t_A$ . The viscous time is  $t_v \approx 10^2 * t_A$  and the magnetic diffusion is  $t_\eta \approx 10^9 * t_A$ . The difference in the evolutions of the kinetic, current, and magnetic helicities can be clearly seen in the first, second, and third panel. These plots show how these quantities grow with the same rate, but different sign, depending on the sign of the initial perturbation, that is, the sign of  $m$ . Note that for each model, the magnetic helicity has an opposite sign to that of the kinetic and current helicities.

Our results are summarized in Table I. We see that the coefficients  $\mu$  and  $\mu_*$  are unchanged for models that differ only in the sign of  $m$  in the perturbation. This is what we expect and one of the symmetries we have used to write the Lagrangian (8). Model He1c shows that the growth rate depends on the value of  $c_s$ , but this does not change the values of  $\mu$  and  $\mu_*$ . Model He1b and model He1d have a smaller growth rate due to a smaller  $v_A/c_s$ . He1b has  $\mu$  and  $\mu_*$  smaller than He1d due to the fact that in the latter model, modes with higher  $k_z$  have been excited by the initial perturbation. Note that in our setup, the ratio  $v_A/c_s$  depends on  $B_0$  but not on  $c_s$ . This is due to the fact that the model is isothermal and the initial radial balance is obtained through a pressure gradient that balances the Lorentz force. An increase of  $n_z$  of the perturbation, as in model He1n10, leads to a similar growth rate, but smaller  $\mu$  and  $\mu_*$ . This can be explained saying that, while in the linear phase this model evolves similarly to any  $n_z = 1$  model, in the weakly nonlinear phase the evolution is different because of a faster growth of modes with higher  $k_z$ . In our models, we measure  $2.2 \leq \mu_*/\mu \leq 2.6$ .

#### IV. HOMOCHIRALITY IN BIOMOLECULES

It is instructive to consider Eqs. (12) as evolution equations for the concentration of two molecules of opposite handedness, L and R. Let us assume that L and R can be synthesized from

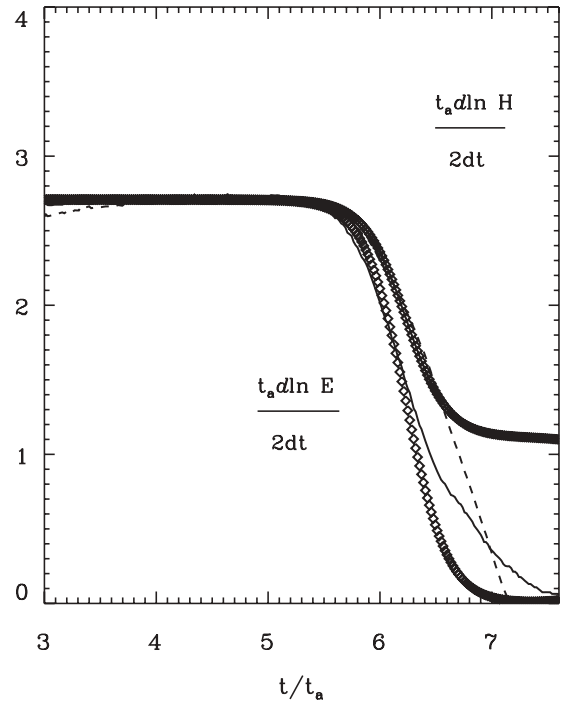
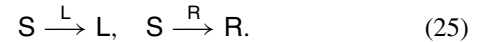
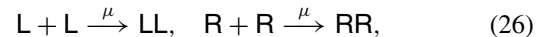


FIG. 5. Time evolution for the logarithmic derivative of kinetic energy (solid line)  $E$  and kinetic helicity  $H$  (dashed) as measured in DNS for models He1 and He1m1 (see Table I).  $t$  is in units of the Alfvén travel time  $t_A$ . We overplot a fit of the model with Eqs. (13). The best fit is obtained for  $\gamma = 2.71/t_A$ ,  $\mu = 7.5t_A/s_{out}^2$ , and  $\mu_* = 18t_A/s_{out}^2$  and the solutions are overplotted on the DNS results.

a substrate **S** through autocatalytic reactions of the form



Autocatalytic reactions of this type have been confirmed in laboratory experiments [28]. Let us assume furthermore that L and R are capable of polymerizing to form homochiral dimers,



as well as heterochiral dimers,



Then the evolution equations for the various concentrations are

$$\frac{d[S]}{dt} = -k_C[S]([L] + [R]), \quad (28a)$$

$$\frac{d[L]}{dt} = k_C[S][L] - 2k_S[L]^2 - 2k_I[L][R], \quad (28b)$$

$$\frac{d[R]}{dt} = k_C[S][R] - 2k_S[R]^2 - 2k_I[L][R], \quad (28c)$$

$$\frac{d[LL]}{dt} = k_S[L]^2, \quad (28d)$$

$$\frac{d[RR]}{dt} = k_S[R]^2, \quad (28e)$$

$$\frac{d[LR]}{dt} = k_I[L][R], \quad (28f)$$

which obeys the conservation law [24]

$$[S] + [L] + [R] + 2[LL] + 2[RR] + 2[LR] = \text{const.} \quad (29)$$

These equations represent a subset of a more general polymerization model [23]. Comparing with Sec. II, we see that Eqs. (28b) and (28c) are *identical* with Eqs. (12a) and (12b) when substituting  $[L] = E_L$  and  $[R] = E_R$ , and identifying

$$k_C = 2\gamma, \quad k_S = 2\mu, \quad k_I = 2\mu_*. \quad (30)$$

Hence we demonstrate quantitatively that the spontaneous production of helicity from the fully nonlinear system of hydromagnetic equations can be described by the simple model equations (12), which in turn represent a simple set of chemical reactions (25)–(27).

The analogy with homochirality in biochemistry is useful because it helps to identify the phenomenon of mutual antagonism as the main cause of chiral symmetry breaking. This effect corresponds to a contribution to the nonlinear terms that result from the interaction between modes of opposite handedness. These are the terms proportional to  $\mu_*$  and  $k_I$  in Eqs. (12) and (28), respectively. In the synthesis of polynucleotides, this is known as enantiomeric cross-inhibition and has been identified in laboratory experiments [29]. The synthesis of heterochiral dimers is essential in that it corresponds to the production of waste needed to eliminate building blocks of that handedness that is later to disappear completely.

## V. CONCLUSIONS

We have shown how net helicity is produced by the addition of a small helical perturbation to a nonhelical system, thus

driving the system to a final state characterized by a finite value of the helicities and, therefore, breaking the initial symmetry. We have shown further that this spontaneous symmetry breaking can be described by weakly nonlinear amplitude equations (13). Furthermore, we have numerically determined the coefficients appearing in the weakly nonlinear amplitude equations (13) for the Tayler instability. Direct numerical simulations show that the ratio between the coefficients describing the weakly nonlinear phase is almost constant. The agreement between the analytical model and the numerical solutions is rather good in the beginning of the weakly nonlinear phase, as shown in Fig. 5. This demonstrates quantitatively the close analogy between helicity production in hydromagnetic flows and the development of homochirality in biochemistry, which is described by the same system of equations as those resulting from the amplitude equations of the weakly nonlinear model of the Tayler instability. It will be useful to extend our analysis by means of a Landau-Ginzburg description of the amplitude equation by including a nonhomogeneous term in our Lagrangian to discuss the possible pattern formation in this type of spontaneous chiral symmetry breaking. We hope to address this issue in a future communication.

## ACKNOWLEDGMENTS

The authors thank P. Chatterjee and M. Rheinhardt for useful discussions. A part of the work was performed when A.B. visited NORDITA under the program “Dynamo, Dynamical Systems and Topology.” F.D.S. acknowledges HPC-EUROPA for financial support. Financial support from European Research Council under the AstroDyn Research Project 227952 is gratefully acknowledged.

- 
- [1] H. Umezawa, *Thermo Field Dynamics and Condensed States* (Elsevier, Amsterdam, 1982).
- [2] N. D. Goldenfeld, *Lectures on Phase Transitions and the Renormalisation Group* (Addison-Wesley, Reading, MA, 1992).
- [3] *Hydrodynamic Instabilities and the Transition to Turbulence*, 2nd ed., edited by H. L. Swinney and J. P. Gollub (Springer-Verlag, New York, 1985); M. C. Cross and P. C. Hohenberg, *Rev. Mod. Phys.* **65**, 851 (1993).
- [4] W. W. Mullins and R. F. Sekerka, *J. Appl. Phys.* **35**, 444 (1964).
- [5] E. Moses and V. Steinberg, *Phys. Rev. A* **34**, 693 (1986); A. J. Simon, J. Bechhoefer, and A. Libchaber, *Phys. Rev. Lett.* **61**, 2574 (1988); G. Faivre, S. de Cheveigne, C. Guthmann, and P. Kurowski, *Europhys. Lett.* **9**, 779 (1989); F. Melo and P. Oswald, *Phys. Rev. Lett.* **64**, 1381 (1990); H. Z. Cummins, L. Fourtune, and M. Rabaud, *Phys. Rev. E* **47**, 1727 (1993).
- [6] J. V. Selinger, Z.-G. Wang, R. F. Bruinsma, and C. M. Knobler, *Phys. Rev. Lett.* **70**, 1139 (1993).
- [7] A. Pinter, M. Lücke, and C. Hoffmann, *Phys. Rev. Lett.* **96**, 044506 (2006).
- [8] P. Chatterjee, D. Mitra, A. Brandenburg, and M. Rheinhardt, *Phys. Rev. E* **84**, 025403(R) (2011); P. Chatterjee, D. Mitra, M. Rheinhardt, and A. Brandenburg, *Astron. Astrophys.* **534**, A46 (2011).
- [9] M. Gellert, G. Rüdiger, and R. Hollerbach, *Mon. Not. R. Astron. Soc.* **414**, 2696 (2011).
- [10] R. J. Tayler, *Mon. Not. R. Astron. Soc.* **161**, 365 (1973).
- [11] R. J. Tayler and P. Markey, *Mon. Not. R. Astron. Soc.* **163**, 77 (1973).
- [12] A. Bonanno and V. Urpin, *Astron. Astrophys.* **477**, 35 (2008).
- [13] A. Bonanno and V. Urpin, *Astron. Astrophys.* **488**, 1 (2008).
- [14] A. Bonanno and V. Urpin, *Phys. Rev. E* **84**, 056310 (2011).
- [15] A. Bonanno and V. Urpin, *Astrophys. J.* **747**, 137 (2012).
- [16] J. Braithwaite and Å. Nordlund, *Astron. Astrophys.* **450**, 1077 (2006).
- [17] J. Braithwaite, *Astron. Astrophys.* **453**, 687 (2006).
- [18] H. Spruit, *Astron. Astrophys.* **349**, 189 (1999).
- [19] S. Fauve, S. Douady, and O. Thual, *J. Phys. II* **1**, 311 (1991).
- [20] F. Quingzeng, *Appl. Math. Mech.* **18**, 865 (1997).
- [21] L. D. Landau and E. M. Lifshitz, *Fluid Mechanics*, Volume 6 of Course of Theoretical Physics, 2nd English ed. (Pergamon, Oxford, 1987), Chap. 3 [Translated from *Gidrodinamika*, 3rd ed., “Nauka”, Moscow, 1986].
- [22] F. C. Frank, *Biochim. Biophys. Acta* **11**, 459 (1953).

- [23] P. G. H. Sandars, *Orig. Life Evol. Biosph.* **33**, 575 (2003).
- [24] A. Brandenburg, A. C. Andersen, S. Höfner, and M. Nilsson, *Orig. Life Evol. Biosph.* **35**, 225 (2005).
- [25] J. Freidberg, *Phys. Fluids* **13**, 1812 (1970).
- [26] J. P. Goedbloed, *Physica* **53**, 535 (1971).
- [27] J. P. H. Goedbloed and S. Poedts, *Principles of Magnetohydrodynamics* (Cambridge University Press, Cambridge, 2004).
- [28] K. Soai, T. Shibata, H. Morioka, and K. Choji, *Nature (London)* **378**, 767 (1995).
- [29] G. F. Joyce, G. M. Visser, C. A. A. van Boeckel, J. H. van Boom, L. E. Orgel, and J. Westrenen, *Nature (London)* **310**, 602 (1984).